ACADEMIC PRESS

Available online at www.sciencedirect.com
SCIENCE DIRECT®

Journal of Colloid and Interface Science 257 (2003) 154–162

JOURNAL OF Colloid and Interface Science

www.elsevier.com/locate/jcis

Small angle neutron scattering study of sodium dodecyl sulfate micellar growth driven by addition of a hydrotropic salt

P.A. Hassan,[1] Gerhard Fritz, and Eric W. Kaler *

Center for Molecular and Engineering Thermodynamics, Department of Chemical Engineering, University of Delaware, Newark, DE 19716, USA

Received 25 January 2002; accepted 18 September 2002

Abstract

The structures of aggregates formed in aqueous solutions of an anionic surfactant, sodium dodecyl sulfate (SDS), with the addition of a cationic hydrotropic salt, *p*-toluidine hydrochloride (PTHC), have been investigated by small angle neutron scattering (SANS). The SANS spectra exhibit a pronounced peak at low salt concentration, indicating the presence of repulsive intermicellar interactions. Model-independent real space information about the structure is obtained from a generalized indirect Fourier transformation (GIFT) technique in combination with a suitable model for the interparticle structure factor. The interparticle interaction is captured using the rescaled mean spherical approximation (RMSA) closure relation and a Yukawa form of the interaction potential. Further quantification of the geometrical parameters of the micelles was achieved by a complete fit of the SANS data using a prolate ellipsoidal form factor and the RMSA structure factor. The present study shows that PTHC induces a decrease in the fractional charge of the micelles due to adsorption at the micellar surface and consequent growth of the SDS micelles from nearly globular to rodlike as the concentration of PTHC increases.

Keywords: Micelles; Small angle neutron scattering; Sphere-to-rod transition; Hydrotropes; Quasielastic light scattering

1. Introduction

The addition of electrolytes to micellar solutions of ionic surfactants can cause the formation of rodlike micelles, and the properties of such micelles depend strongly on the molecular structure of the counterions [1–10]. The self-assembly of surfactant molecules in aqueous solutions is governed by a balance between opposing forces. The main driving force is reduction of the unfavorable water–hydrocarbon interfacial energy, while counteracting forces arise from the steric and electrostatic interactions that result from bringing the charged head groups into close proximity and the associated diffuse layer of counterions. The electrostatic contribution to the free energy of formation of micelles can be influenced by the addition of electrolytes or cosurfactants. Conventional electrolytes influence the electrostatic free energy by mixing with the counterions while cosurfactants may influence the free energy by a decrease of the surface charge density. Typically, addition of substantial quantities of inorganic electrolytes is necessary to induce the formation of rodlike micelles [5]. However, only millimolar quantities of hydrotropic salts are sufficient to induce the transition from spherical to rodlike micelles [7]. Appropriate hydrotropic salts contain aromatic counterions that adsorb on the surfaces of the micelles and thereby decrease their surface charge density. In addition, the co-ion released by ionization of the hydrotropic salt increases the ionic strength and screens electrostatic interactions.

There are many studies of the formation and properties of rodlike micelles formed by cationic surfactants upon addition of aromatic counterions such as salicylate, tosylate, and naphthalene carboxylate [9]. Analogous reports of anionic surfactant micelles are very limited, despite their industrial uses, although we have recently reported a sphere-to-rod transition for sodium dodecyl sulfate (SDS) micelles in the presence of a hydrotropic salt, *p*-toluidine hydrochloride (PTHC), at less than equimolar ratios of salt to surfactant [11]. The hydrotropic salt PTHC, being a strong electrolyte, dissociates in water to form *p*-toluidinium cation (PTH^+) and Cl^- anion. The cationic nature of PTH^+ facilitates the adsorption of the ion to the negatively charged

* Corresponding author.
E-mail address: kaler@che.udel.edu (E.W. Kaler).
[1] Permanent address: Novel Materials and Structural Chemistry Division, Bhabha Atomic Research Centre, Mumbai, India.

0021-9797/03/$ – see front matter
PII: S0021-9797(02)00020-6

SDS micelle surface. The adsorption and orientation of the PTH^+ on SDS micelle surface was confirmed from previous NMR studies [11]. Note that the neutral analog of this salt, *p*-toluidine, is highly insoluble in water and in the presence of SDS micelles and so does not induce any significant micellar growth. The present report details the changes in structure and interactions of SDS micelles with the addition of the hydrotropic salt PTHC as revealed by SANS measurements.

2. Materials and methods

Sodium dodecyl sulfate (electrophoresis grade) was purchased from Fisher Scientific and *p*-toluidine hydrochloride was obtained from Aldrich. All chemicals were used as received. Stock solutions of SDS and PTHC were prepared in D_2O (Cambridge Isotopes) and mixed in varying ratios.

Small angle neutron scattering (SANS) experiments were performed using the NG-7 spectrometer at the Cold Neutron Research Facility of the National Institute of Standards and Technology (NIST) in Gaithersburg, MD. The incident neutron wavelength was 6 Å. Samples were held in quartz cells with 2-mm path lengths and maintained at 25 °C. Measurements were made at different sample-to-detector distances to cover a scattering vector (q) range of 0.005 to 0.6 $Å^{-1}$. The scattering spectra were corrected for background scattering, empty cell contributions, sample transmission, and detector efficiency, and the corrected data were radially averaged and placed on an absolute scale using NIST protocols and calibration standards. The incoherent background was determined by Porod extrapolation of the data in the high-q region and was subtracted before data evaluation. Corrections due to finite instrumental resolution were taken into account throughout the data evaluation. In the model scattering curves, the calculated intensities were smeared by convoluting with a Gaussian resolution function at each scattering vector. The quality of the fits is assessed from the reduced χ^2 values [12].

3. Data analysis

There are two general approaches to the analysis of SANS data. One is the model-independent indirect Fourier transformation (IFT) [13] of the experimental scattering curve to obtain the pair distance distribution function (PDDF) $p(r)$, and the second is the direct modeling of the structure with an appropriate form and comparison of the calculated scattering curve for the model with the experimental data. The IFT method can be applied to any spectrum and it transforms the scattering curve into real space information. Interpretation of the results is limited to the cases where interparticle interactions can be neglected. However, this method has been extended to a generalized indirect Fourier transformation (GIFT) [14] method wherein a model for the interparticle structure factor is assumed and is incorporated into the IFT. The GIFT method separates the form factor (intraparticle) and the structure factor (interparticle) scattering and uses the same model-free approach to calculate the PDDF that corresponds only to the form factor. In the case of monodisperse, spherical scatterers the PDDF, $p(r)$, is related to the differential scattering cross section per unit volume ($d\Sigma/d\Omega$) by

$$\frac{d\Sigma(q)}{d\Omega} = NS(q)4\pi \int_0^\infty p(r)\frac{\sin(qr)}{qr}\,dr, \tag{1}$$

where N is the number density of the micelles and $S(q)$ is the interparticle structure factor. Considering the instrumental smearing effects due to finite resolution, the experimental scattered intensity, $I(q)$, can be related to the cross section by

$$I(q) = \int R(q)\frac{d\Sigma(q)}{d\Omega}\,dq, \tag{2}$$

where $R(q)$ is the resolution function. Structural information about the scatterers can be assessed from the $p(r)$ function because it is directly connected to the convolution square of the scattering contrast profile. One important parameter readily obtained from the $p(r)$ function is the maximum dimension of the scatterers.

In the case of cylindrical particles, when the length is much larger than the diameter, it is possible to obtain the cross section PDDF, $p_c(r)$, by separating the effects of the length and cross section. Again, from the $p_c(r)$ the maximum diameter of the micelle can be assessed.

Information from the PDDF can be supplemented to construct a suitable model that can be fitted to the experimental scattering curve. Because the model independent analysis shows that the micelles undergo a transition from globular to rodlike objects, a prolate ellipsoidal form factor in conjunction with a suitable structure factor is used to model the experimental data directly.

The differential scattering cross section per unit volume ($d\Sigma/d\Omega$) for a system of monodisperse interacting anisotropic particles can be written as [15]

$$d\Sigma(q)/d\Omega = NP(q)S'(q), \tag{3}$$

where $S'(q)$ is the orientationally averaged structure factor. For an ellipsoidal micelle with semimajor axis a and semiminor axis b, the form factor $P(q)$ is [15]

$$P(q) = \int_0^1 \left|F(q,\mu)\right|^2 d\mu, \tag{4}$$

$$F(q,\mu) = v(\rho_m - \rho_s)\frac{3j_1(u)}{u},$$
$$u = q\left[a^2\mu^2 + b^2(1-\mu^2)\right]^{0.5}, \tag{5}$$

where v is the volume of the micelle, ρ_m and ρ_s are the coherent scattering length densities of the micelle and solvent,

respectively, and $j_1(u)$ is the first order spherical Bessel function. The orientationally averaged structure factor $S'(q)$ is related to the structure factor for an equivalent solution of spherical micelles $S(q)$ by [15]

$$S'(q) = 1 + \frac{\langle F(q,\mu)\rangle^2}{\langle |F(q,\mu)|^2\rangle}\big(S(q) - 1\big). \tag{6}$$

The interparticle structure factor $S(q)$ specifies the correlation between the centers of different particles. $S(q)$ has been evaluated analytically for charged spherical particles by Hayter and Penfold using the mean spherical approximation [16]. Later these results have been extended to dilute charged colloidal dispersions by a rescaled mean spherical approximation (RMSA) procedure [17]. We used the RMSA expressions together with the Yukawa form of the potential between the micellar "macro-ions" to account for the interparticle interactions.

The number of free parameters required to fit the data were restricted as follows. The micelle number density can be calculated from the concentration of micelles and the volume occupied by one surfactant monomer, assuming no volume change on mixing. The surfactant monomer volume has been estimated by Tanford [18]. With the addition of hydrotropic salt a small but appreciable change in the volume fraction of the micelle is expected as the salt is solubilized into the micelle surface. The volume occupied by the hydrotrope molecules is included in the volume fraction of the micelles, reflecting the assumption that all the hydrotrope molecules are solubilized in the micelles. Because of the penetration of water molecules into the headgroup region of the micelles, the scattering length density of the headgroup region is not significantly different from that of solvent. Thus the minor radius (b) of the ellipsoid is initially held at the length of the hydrocarbon chain (16.7 Å) at low salt concentrations. At higher salt concentrations, where there is no peak observed in the spectra, the quality of the fits was improved by use of a slightly higher value of the minor radius. The maximum value of the minor radius used is 18.2 Å, which is only slightly different from the initial value.

The interparticle structure factor $S(q)$ is governed by the volume fraction and surface charge of the micelles and the ionic strength of the medium. The ionic strength is fixed by the concentration of unassociated surfactant molecules and the counterions arising from the added hydrotropes. In the RMSA procedure, it is assumed that ellipsoidal micelles behave as a rigid equivalent sphere with diameter $\sigma = 2(ab^2)^{1/3}$ interacting through a screened Coulomb potential. Thus the two adjustable parameters used to fit the data are the semimajor axis (a) of the ellipsoid and the surface charge of the micelles. A similar approach has been used in the evaluation of SANS measurements of other micellar solutions [4,15,19–21]. Any accounting of the polydispersity of the micelles and/or elliptical cross section of the micelles will introduce additional parameters and is not done here, although the question of cross section is discussed below.

4. Results and discussion

Figure 1 shows the SANS spectra of 50 mM SDS in presence of various amounts of PTHC. The molar ratio of PTHC to SDS in the sample (x_{PTHC}) is varied from 0 to 0.6, beyond which the solution becomes turbid due to the strongly associative nature of the salt and surfactant. We believe that the formation of a catanionic salt near the equimolar ratio is responsible for the appearance of turbidity in the solution beyond $x_{\mathrm{PTHC}} = 0.6$. In the case of cationic micelles such as cetyl trimethyl ammonium bromide (CTAB) with the addition of sodium salicylate [7], no such turbidity is observed even at a very high ratio of salt to surfactant. This is probably due to the greater length of the hydrocarbon chains in CTAB (C_{16}) than in SDS (C_{12}). The larger asymmetry of the hydrocarbon chain lengths in oppositely charged surfactant–additive pairs prevents the precipitation of catanionic salt. This is also evident from the difference in aggregation behavior of cetyltrimethyl ammonium alkyl sulfonate ($CTAC_nSO_3$) surfactants [22]. For $n = 6$ or 7 isotropic viscoelastic phases exist at low surfactant concentrations, whereas for $n = 8$ the aggregates are vesicles. A similar turbid region is observed in the phase behavior of the SDS–octyl trimethylammonium bromide (C_8TAB)–water system [23]. Addition of a larger hydrophobic counterion such as hydroxynaphthalene carboxylate (HNC^-), the naphthalene analog of salicylate, to CTAB also produces a turbid phase near the equimolar ratio, while no such phase is observed with salicylate [24].

The spectra in Fig. 1 clearly distinguish two different regimes: $x_{\mathrm{PTHC}} \leqslant 0.3$, where a correlation peak occurs, and $x_{\mathrm{PTHC}} > 0.3$, where the peak vanishes. The presence of a peak is an indication of strong repulsive intermicellar interactions and this effect is captured by $S(q)$. As $q \to 0$, $S(q)$ becomes proportional to the osmotic compressiblity of the solution, which is quite low. At low salt concentrations ($x_{\mathrm{PTHC}} \leqslant 0.3$), the scattering curves show correlation peaks indicating the presence of a repulsive electrostatic interaction. At high values of q, $S(q) \to 1$, and the intensity is dominated by $P(q)$.

With increasing x_{PTHC}, there is a broadening of the interaction peak suggesting a screening of the electrostatic interaction. The strength of this repulsive interaction is set by the surface charge and the ionic strength of the medium. Addition of a salt increases the ionic strength and hence decreases the range of electrostatic interactions. Similar effects are observed in ionic micelles in the presence of large amounts of inorganic electrolytes, but they are seen here after the addition of a small amount of PTHC because of incorporation of the PTHC into the surface of the micelles and a concomitant decrease in the surface charge density of the micelles. There is also a slight shift of the peak to lower q as x_{PTHC} increases, suggesting an increase of the average intermicellar distance, which would correspond to an increase in the aggregation number of the micelles.

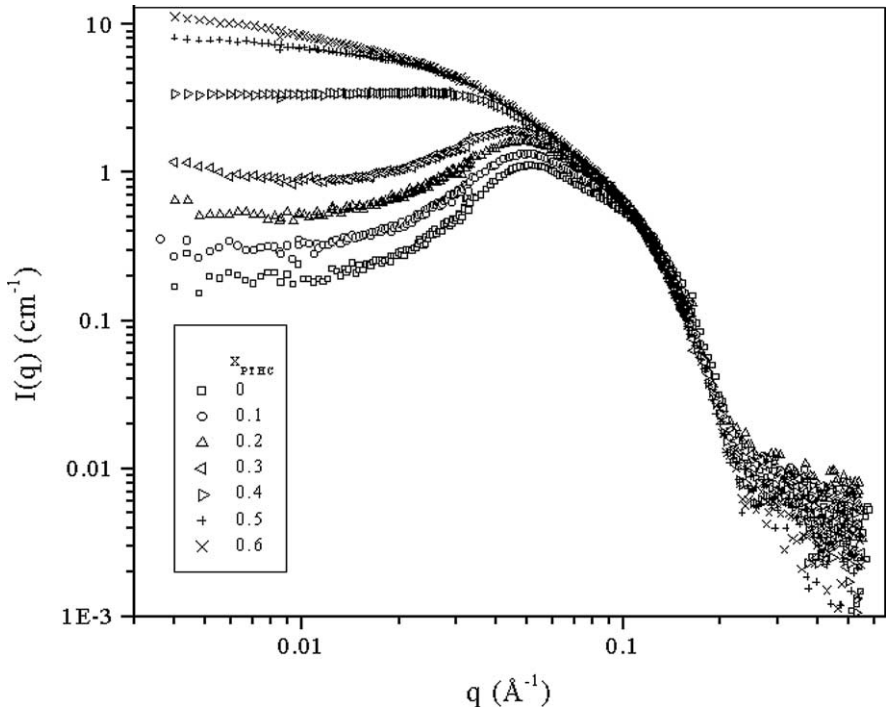

Fig. 1. Scattering intensity, $I(q)$ as a function of scattering vector q for 50 mM SDS with various amounts of added salt PTHC. The molar ratio of salt to surfactant is indicated as x_{PTHC}.

When x_{PTHC} is above 0.3, the peaks in the spectra vanish. The disappearance of the correlation peak by addition of a few millimoles of the salt clearly indicates a decrease of the intermicellar interactions. This is due to the adsorption of the counterion on the surface of the micelles and subsequent neutralization of the charge on the micelles. This surface charge decrease also lowers the average area occupied by the surfactant head group, and closer head group packing makes rodlike micelles more energetically favorable [25]. The SANS spectra at high-q regions virtually merge for all salt concentrations, indicating that the smallest dimension of the micelles remains approximately the same for all values of x_{PTHC}.

We begin our analysis of the scattering spectra by the IFT method. Figure 2 shows the results of IFT calculations without considering interparticle interactions, and, as expected, the oscillations of the calculated $p(r)$ curves clearly demonstrate that intermicellar interactions cannot be neglected. For $x_{\mathrm{PTHC}} \leqslant 0.3$ the $p(r)$ function goes through a negative minimum and shows strong oscillations that vanish at very long distances. The presence of these oscillations is a clear signature of the presence of intermicellar interactions [26]. The strength of these oscillations decreases for $x_{\mathrm{PTHC}} = 0.4$ and a rapid increase in the maximum dimension of the aggregates is found for $x_{\mathrm{PTHC}} = 0.5$ and 0.6. The $p(r)$ function for $x_{\mathrm{PTHC}} = 0.5$ and 0.6 resembles that of a mixture of short rods and long rods with two well-separated distributions. However, because it is unlikely there is a bimodal distribution of micellar sizes, this feature probably arises from the contribution of weak intermicellar interactions.

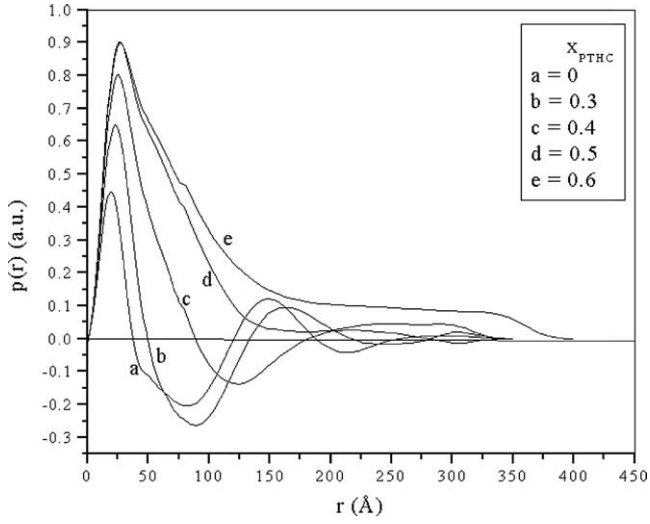

Fig. 2. Pair distance distribution functions, $p(r)$, obtained from the IFT of the SANS spectra without considering any interparticle interactions for 50 mM SDS at different values of x_{PTHC}.

Since the IFT evaluations indicated the presence of interactions, GIFT evaluations were carried out incorporating a suitable model of the structure factor. There are different approximate closure relations for evaluating the structure factor using the Ornstein–Zernike equation. A commonly used closure relation for the analysis of SANS data of micellar solutions is the rescaled mean spherical approximation (RMSA) [16,17]. Another widely used closure relation is the hypernetted-chain (HNC) approximation, which is accurate when long-range interactions are important. A more thermo-

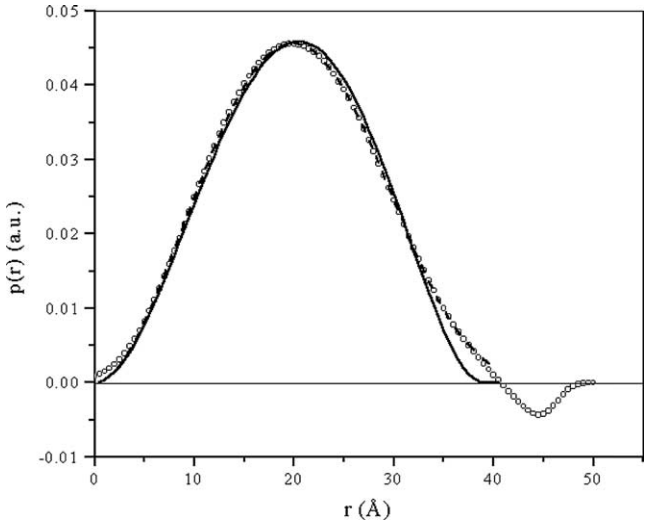

Fig. 3. One representative pair distance distribution function $p(r)$ obtained from GIFT analysis with the interparticle interaction described by the RMSA closure (50 mM SDS, no salt). The solid line is the $p(r)$ calculated by a convolution square of the contrast profile for homogenous mondisperse spheres having radius 19.5 Å, while the dashed line is calculated for a polydisperse population of spheres with an average radius of 17.9 Å and 15% polydispersity.

Table 1
Comparison of the results from different closure relations used in the GIFT evaluation of SANS spectra (50 mM SDS, no added salt)

Closure relation	Radius (Å)	Charge (e)	$D_{max}/2$ (Å)
RMSA	19	30	21
HNC	19	35	21
RY	19	32	21

D_{max} is the point where the $p(r)$ function goes to zero.

dynamically self-consistent closure relation is that of Rogers and Young (RY) [27], which mixes the different approximations valid for short- and long-range interactions.

The $p(r)$ function for $x_{PTHC} = 0$ evaluated with the GIFT method when the interactions are taken into account using the RMSA procedure is shown in Fig. 3. In the structure factor calculations only the charge on the micelle and its diameter are varied. To check the accuracy of the RMSA procedure, the results of RMSA calculations are compared with those of the HNC and RY closure relations (Table 1). The values are not significantly different for RMSA or RY closures, so the simpler RMSA closure is used to reduce computational complexity.

The shape of the $p(r)$ function in Fig. 3 is similar to that expected for globular particles. The contrast profile of the scattering objects can be directly assessed from the $p(r)$ by a deconvolution procedure. The $p(r)$ functions calculated using the convolution square of an assumed contrast profile for monodisperse or polydisperse homogeneous spheres were compared with the $p(r)$ obtained from GIFT analysis (Fig. 3). The solid line in Fig. 3 indicates the best fit with a monodisperse homogeneous sphere with radius 19.5 Å, while the dashed line corresponds to the fit with polydisperse

Table 2
Results from the GIFT analysis of the SANS spectra of samples with x_{PTHC} 0 to 0.3, using RMSA closure for structure factor

x_{PTHC}	r_{mono} (Å)	Mean r (Å)	Polydispersity (%)	$D_{max}/2$ (Å)
0	20	18	15	21
0.1	21	19	15	22
0.2	22	19	20	24
0.3	24	17	35	30

r_{mono} is the optimum radius from the convolution square of contrast profile assuming mondisperse spheres and mean r and polydispersity are the parameters assuming polydisperse homogeneous spheres. D_{max} is the point where the $p(r)$ function goes to zero.

homogeneous spheres having a mean radius of 17.9 Å and 15% polydispersity (assuming a Schultz distribution of particle size). Not surprisingly, the observed $p(r)$ function is fitted better with a polydisperse sphere model. For $x_{PTHC} \leqslant 0.3$, the shape of the $p(r)$ function remains the same as that shown in Fig. 3 except that the maximum dimension of the micelles increases slightly. The results of the average size and polydispersity and the maximum dimension are summarized in Table 2.

For $x_{PTHC} = 0.4$ the shape of the $p(r)$ function is similar to that expected for cylindrical particles [26]. In this case $p(r)$ is similar to that for spheres at small values of r but then shows a pronounced maximum. Beyond the maximum there is an inflection point, after which the function decays linearly to zero. The onset of a linear decay in $p(r)$ is clear indication of the formation of elongated micelles. A similar profile is observed for $x_{PTHC} = 0.5$ with a higher maximum dimension for the micelles. However, no numerically stable solution could be obtained from the GIFT evaluation for $x_{PTHC} = 0.6$. This could be because of the failure of the model used for the structure factor in the case of such elongated micelles. The results, however, clearly demonstrate that the micelles are elongated and increase in length as x_{PTHC} increases.

For anisotropic micelles, the cross sectional structure can be directly assessed from an IFT of the spectra at high q. The cross sectional PDDF, $p_c(r)$, for a cylindrical particle having length L much greater than the diameter d is related to the scattering cross section by the relation [26]

$$\frac{d\Sigma(q)}{d\Omega} = \frac{2\pi^2 L}{q} \int_0^\infty p_c(r) J_0(qr)\, dr, \tag{7}$$

where J_0 is the zeroth order Bessel function. Since the cross sectional PDDF is calculated from the high-q region of the spectra, the effect of interparticle interaction is negligible, and the low-q portion of the spectra is not included in the analysis. For cylindrical particles, the low-q cut-off is determined from a Guinier plot of $\ln(I(q)q)$ vs. q^2 because the portion of the scattering curve corresponding to the cross section leads to a linear decay on a Guinier plot (see Fig. 4 inset).

Figure 4 shows the $p_c(r)$ function for $x_{PTHC} = 0.6$ and the corresponding fits with monodisperse and poly-

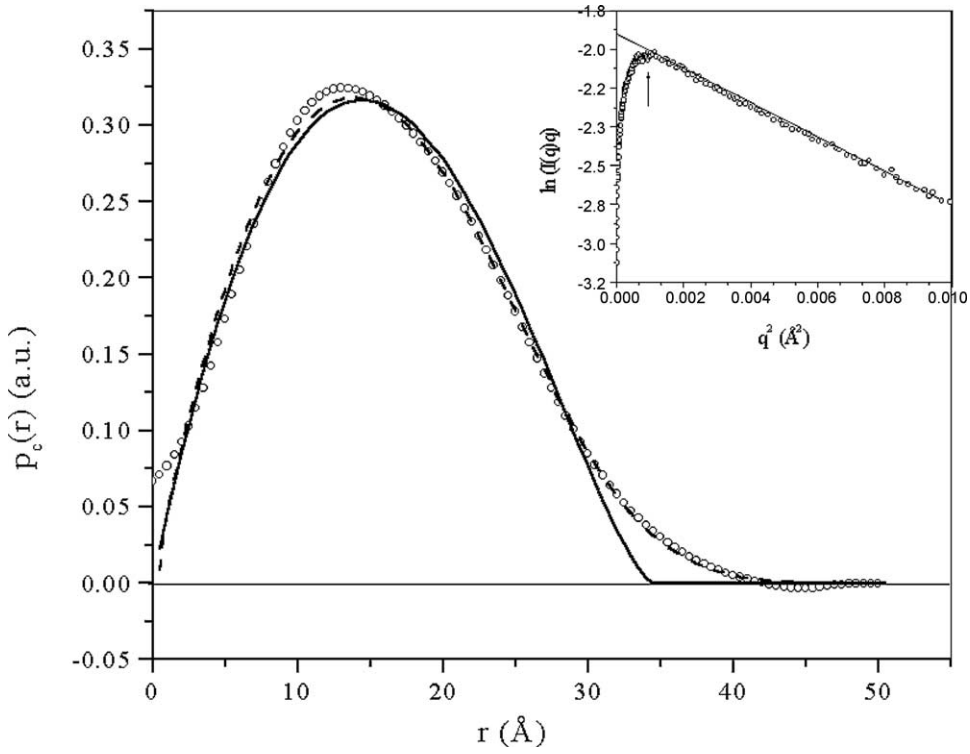

Fig. 4. A representative cross section PDDF, $p_c(r)$, obtained from IFT of the high-q region of the SANS spectra ($x_{PTHC} = 0.6$). The solid line is the $p_c(r)$ calculated by a convolution square of the contrast profile for homogenous mondisperse circular cross section having radius 17.3 Å, while the dashed line represents the $p_c(r)$ for a polydisperse circular cross section with an average radius of 15.6 Å and 20% polydispersity. The inset shows the cross sectional Guinier plot indicating a linear decay at the high-q region. The low-q cutoff is shown by the arrow.

Table 3
Results from the cross sectional PDDF of SANS spectra of samples with x_{PTHC} 0.4 to 0.6

x_{PTHC}	r_{mono} (Å)	Mean r (Å)	Polydispersity (%)	$D_{max}/2$ (Å)
0.4	17	16	17.5	20
0.5	17	16	17.5	21
0.6	17	16	20	21

r_{mono} is the optimum radius from the convolution square of contrast profile assuming a monodisperse circular cross section and mean r and polydispersity are the parameters assuming polydisperse circular cross sections. D_{max} is the point where the $p_c(r)$ function goes to zero.

disperse circular cross sections. The results of the cross sectional analysis of samples with $x_{PTHC} > 0.3$ are summarized in Table 3. The better agreement of the data with a polydisperse cross section is almost certainly because the long anisotropic micelles have elliptical cross sections. Recent SANS studies have clearly shown the presence of elliptical cross sections in long micelles made from SDS and dodecyl trimethyl ammonium bromide (DTAB) in the presence of added salt [28,29].

Quantitative estimates of the micellar parameters were obtained by fitting the entire SANS spectra with an assumed model. GIFT evaluations clearly suggest a growth of the micelles from nearly globular objects to long anisotropic micelles. Thus a prolate ellipsoidal form factor with a circular cross section is used to fit the data together with the RMSA closure for structure factor. The semimajor axis of the ellipsoid (a) and the surface charge of the micelle are varied and the same form factor could be used at all salt concentrations from $x_{PTHC} = 0$ to 0.6. It might be more realistic under some conditions to use other models since, for example, it has been shown that SDS micelles in the absence of salts can best be described as oblate ellipsoids and the longer micelles formed by the addition of salt have an elliptical cross section [28]. However, any accounting for these factors will introduce additional parameters into the fit and will influence only the high-q region of the spectra where the standard errors in the data are higher. In addition, the maximum cross sectional radius of the long micelles, as seen from the $p_c(r)$ function, is 21 Å. This is only 4.3 Å higher than the length of the hydrocarbon chain of the SDS molecule (16.7 Å). Micelles are dynamic species, so small shape fluctuations and diffuse longitudinal correlations are likely and will introduce a small polydispersity in the circular cross section. The adsorption of the hydrotropic salt PTHC on the surface of the SDS micelles can increase the scattering contrast of the head group region compared to that of sulfate groups and can lead to a cross section radius slightly larger than 16.7 Å. The limited resolution of the data in the high-q region will make it difficult to differentiate these effects in direct model fitting, so the simpler ellipsoid model was chosen.

The scattering data, together with the model fits, for SDS samples with different hydrotrope concentrations are given

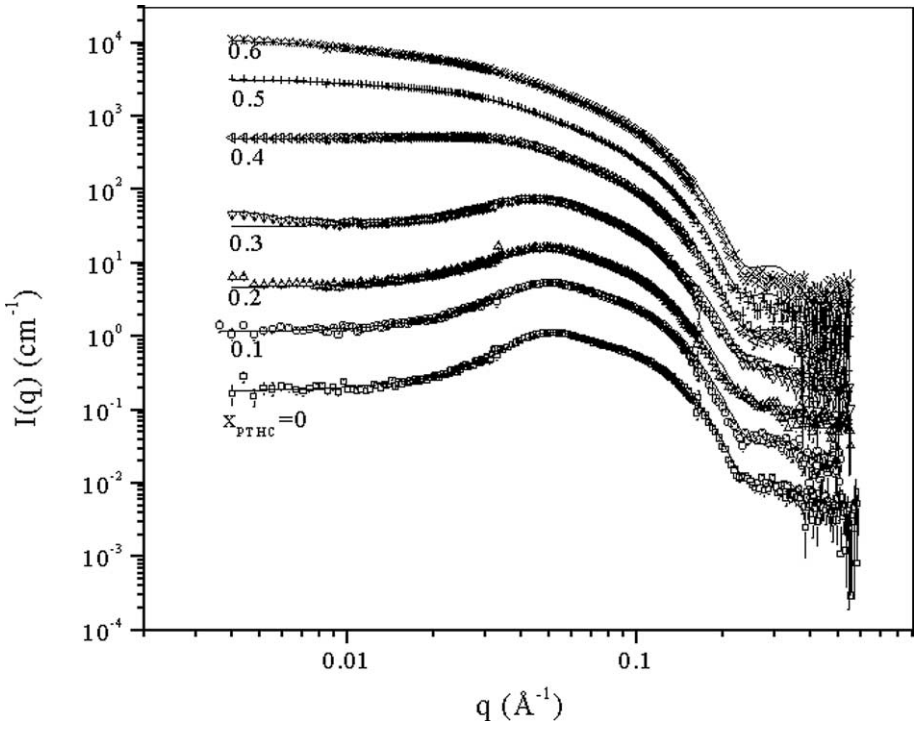

Fig. 5. SANS spectra in Fig. 1 and the corresponding fit to the data using a prolate ellipsoid form factor and a RMSA structure factor. The spectra are shifted for clarity. The reduced χ^2 of the model fits and the corresponding x_{PTHC} in parentheses are as follows: 4.0 (0), 6.3 (0.1), 14.9 (0.2), 20.4 (0.3), 6.1 (0.4), 8.7 (0.5), 26.1 (0.6).

Table 4
Micellar parameters obtained from the fits of the complete SANS curve using a prolate ellipsoidal form factor and the RMSA closure for the structure factor

x_{PTHC}	Aggregation number (N_{agg})	Fractional charge (α)	Semiminor axis, b (Å)	Semimajor axis, a (Å)
0	79 ± 1	0.42 ± 0.13	16.7	25 ± 2.1
0.1	92 ± 8	0.36 ± 0.08	16.7	30 ± 2.7
0.2	109 ± 11	0.31 ± 0.09	16.7	37 ± 3.7
0.3	131 ± 12	0.25 ± 0.07	16.7	47 ± 4.4
0.4	261 ± 7	0.1 ± 0.01	17.8	95 ± 2.4
0.5	565 ± 16	0.12 ± 0.01	18.2	213 ± 6
0.6	721 ± 41	0.1 ± 0.01	17.7	281 ± 16

The standard errors on the parameters are estimated as the values for which the χ^2 increases to twice the value at χ^2 minimum.

in Fig. 5. At low salt concentrations the micelles appear to be somewhat globular and with successive addition of the salt the micelle size increases. The results from the model fits are summarized in Table 4. The aggregation number of the micelle is estimated from the volume of the ellipsoid and the volume occupied by surfactant and hydrotrope molecules. The fractional charge is estimated from the ratio of surface charge of the micelles to the aggregation number. Figure 6 shows the micelle aggregation number (N_{agg}), the fractional charge on the micelle (α), and the semimajor axis (a) as functions of salt concentration. The results suggest that, assuming a prolate ellipsoidal structure to the micelles having a semiminor axis of 16.7 Å, the semimajor axis increases slowly from 25 to about 47 Å as x_{PTHC} approaches 0.3, above which the micelles grow rapidly. It is evident from previous studies that the aggregation numbers of SDS micelles in 0.1 M NaBr estimated using oblate and prolate ellipsoidal models agrees well irrespective of the model for form factor [28].

The aggregation number observed for SDS micelles in the absence of any added salt is in good agreement with those reported earlier [4–6]. The micelle aggregation number initially increases slowly upon the addition of PTHC until x_{PTHC} is above 0.3, whereupon N_{agg} increases more dramatically. Similarly, the fractional charge on the micelle initially decreases quickly and then reaches a steady value. The calculated spectra $I(q)$ are very sensitive to the changes in the aggregation number, but are only weakly sensitive to the value of the fractional charge. Nevertheless, it is clear from the disappearance of the peak that the effective charge on the micelle decreases with the addition of salt and this trend is effectively captured in the estimated parameter. Moreover, at sufficiently high salt concentrations the micelles become elongated and thus the decoupling approximation used to estimate the structure factor of anisotropic particles becomes less reliable.

Another notable feature of the spectra at the intermediate salt concentration ($x_{PTHC} = 0.3$) is that the scattering curve at low q shows a small increase (see the correspondingly high value of χ^2). This could be an indication of attractive interactions between the micelles. It is unlikely that this attraction is due only to the van der Waals interactions as a similar increase is not observed at higher x_{PTHC}.

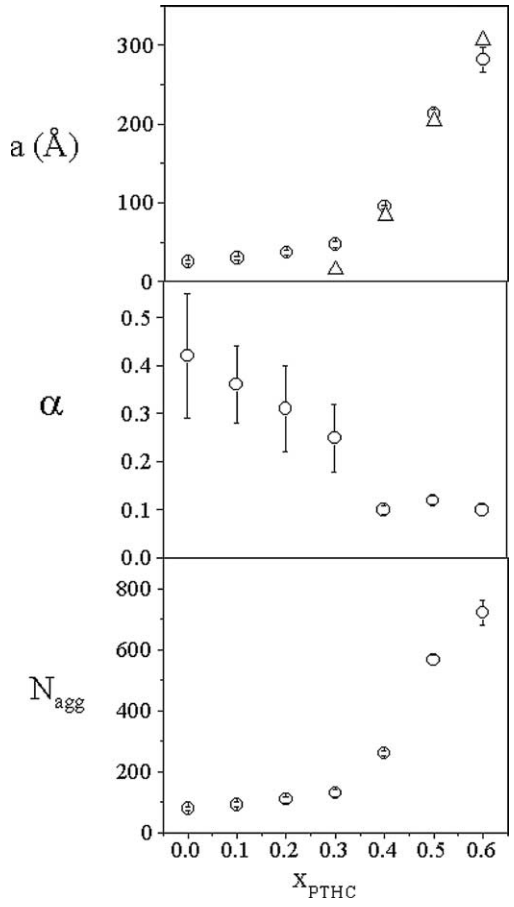

Fig. 6. Variation of aggregation number (N_{agg}), fractional charge (α), and semimajor axis (a) of SDS micelles as a function of x_{PTHC}. The open triangles represent data from QLS measurements [11].

Mixtures of rods and spheres do show an entropy-driven depletion interaction [30,31], and it is perhaps possible that such a rod/sphere mixture could exist at intermediate salt concentrations and give rise to this scattering feature.

Finally, when intermicellar interactions are screened by a sufficient amount of electrolyte, the intensity at low q values increases. QLS measurements were made on these samples [11] and the length of the micelle is evaluated after correcting for possible hydrodynamic and osmotic contributions. Reasonably good agreement is found between the two independently measured values (Fig. 6). This confirms the picture that the micelles undergo uniaxial growth from spheres to rodlike objects.

5. Conclusions

The growth of SDS micelles by the addition of a hydrotropic salt at less than equimolar concentrations is established from SANS measurements. A strong repulsive interaction between the micelles at low salt concentrations is evident from the presence of a correlation peak in the spectra. The evolution of the spectra clearly indicates a decrease of the electrostatic interaction and a uniaxial growth of the micelles. The generalized indirect Fourier transformation of the data suggests that the micelles are nearly globular at low salt concentrations and become elongated as salt concentration increases. Further, it suggests that the cross section of the elongated micelles is elliptical rather than circular. The micellar parameters were evaluated by assuming a prolate ellipsoidal growth and employing the Yukawa potential within the RMSA procedure. A drastic decrease of the surface charge and a corresponding increase in aggregation number is observed as salt is added. The decrease of the surface charge at less than equimolar ratios of salt indicates that the salt is strongly adsorbed on the surface of the micelles. When the surface charge density becomes sufficiently low, the micelles grow rapidly. The lengths of the micelles evaluated from SANS measurements are consistent with the results from previous quasielastic light scattering measurements.

Acknowledgments

The authors acknowledge the support of the National Institute of Standards and Technology, US Department of Commerce, for the use of neutron research facilities. We are also thankful to J.A. Silas, B. Baser, and M. Labourt-Ibarre for assistance. We thank Dr. Steve Kline (NIST) for many fruitful discussions. This work was supported by the National Science Foundation (CTS-9814399).

References

[1] N.A. Mazer, G.B. Benedek, M.C. Carey, J. Phys. Chem. 80 (1976) 1075.
[2] G. Porte, J. Appell, J. Phys. Chem. 85 (1981) 2511.
[3] F. Kern, P. Lemarechal, S.J. Candau, M.E. Cates, Langmuir 8 (1992) 437.
[4] V.K. Aswal, P.S. Goyal, Phys. Rev. E 61 (2000) 2947.
[5] L.J. Magid, Z. Li, P.D. Butler, Langmuir 16 (2000) 10028, and references therein.
[6] S.H. Chen, Annu. Rev. Phys. Chem. 37 (1986) 351, and references therein.
[7] H. Rehage, H. Hoffmann, Mol. Phys. 74 (1991) 933.
[8] M.E. Cates, S.J. Candau, J. Phys. Condensed Matter 2 (1990) 6869.
[9] L.J. Magid, J. Phys. Chem. 102 (1998) 4064.
[10] R.T. Buwalda, M.C.A. Stuart, J.B.F.N. Engberts, Langmuir 16 (2000) 6780.
[11] P.A. Hassan, S.R. Raghavan, E.W. Kaler, Langmuir 18 (2002) 2543.
[12] J.S. Pedersen, Adv. Colloid Interface Sci. 70 (1997) 171.
[13] O. Glatter, J. Appl. Crystallogr. 10 (1977) 415.
[14] J. Brunner-Popela, O. Glatter, J. Appl. Crystallogr. 30 (1997) 431.
[15] E.Y. Sheu, C.F. Wu, S.H. Chen, J. Phys. Chem. 90 (1986) 4179.
[16] J.B. Hayter, J. Penfold, Mol. Phys. 42 (1981) 109.
[17] J.P. Hansen, J.B. Hayter, Mol. Phys. 46 (1982) 651.
[18] C. Tanford, The Hydrophobic Effect: Formation of Micelles and Biological Membranes, 2nd ed., Wiley, New York, 1980.
[19] S.S. Berr, J. Phys. Chem. 91 (1987) 4760.
[20] D. Bendedouch, S.H. Chen, W.C. Koehler, J. Phys. Chem. 87 (1983) 2621.

[21] F. Quirion, L.J. Magid, J. Phys. Chem. 90 (1986) 5435.
[22] R. Oda, J. Narayanan, P.A. Hassan, C. Manohar, R.A. Salkar, F. Kern, S.J. Candau, Langmuir 14 (1998) 4364.
[23] C.A. Barker, D. Saul, G.J.T. Tiddy, B.A. Wheeler, E. Willis, J. Chem. Soc. Faraday Trans. 1 70 (1974) 154.
[24] B.K. Mishra, S.D. Samant, P. Pradhan, S.B. Mishra, C. Manohar, Langmuir 9 (1993) 894.
[25] J.N. Israelachvili, D.J. Mitchell, B.W. Ninham, J. Chem. Soc. Faraday Trans. 2 72 (1976) 1525.
[26] O. Glatter, in: P. Lindner, Th. Zemb (Eds.), Neutron, X-Ray and Light Scattering, North-Holland, Amsterdam, 1991.
[27] F.J. Rogers, D.A. Young, Phys. Rev. A 30 (1984) 999.
[28] M. Bergstrom, J.S. Pedersen, Phys. Chem. Chem. Phys. 1 (1999) 4437.
[29] M. Bergstrom, J.S. Pedersen, J. Phys. Chem. B 103 (1999) 8502.
[30] X. Ye, T. Narayanan, P. Tong, J.S. Huang, Phys. Rev. Lett. 76 (1996) 4640.
[31] K. Lin, J.C. Crocker, A.C. Zeri, A.G. Yodh, Phys. Rev. Lett. 87 (2001) 088301.